Sustainable Energy & Fuels

Sustainable one step process of making carbon-free TiO2 anode and sodium-ion battery electrochemistry

Journal:	*Sustainable Energy & Fuels*
Manuscript ID	SE-ART-02-2018-000082.R2
Article Type:	Paper
Date Submitted by the Author:	10-May-2018

Complete List of Authors:	Chadha, Tandeep; Washington University in St. Louis, Energy, Environmental and Chemical Engineering Dutta, Prasit; Indian Institute of Technology Bombay, Department of Energy Science and Engineering Raliya, Ramesh; Washington University in St. Louis, Energy, Environmental and Chemical Engineering Mitra, Sagar; Indian Institute of Technology Bombay, Department of Energy Science and Engineering Biswas, Pratim; Washington University in St Louis, Energy, Environmental and Chemical Engineering

Journal Name

ARTICLE

Sustainable one step process of making carbon-free TiO_2 anode and sodium-ion battery electrochemistry

Received 00th January 20xx,
Accepted 00th January 20xx

DOI: 10.1039/x0xx00000x

www.rsc.org/

Tandeep S. Chadha[a,#], Prasit Kumar Dutta[b,#], Ramesh Raliya[a], Sagar Mitra[b,*], Pratim Biswas[a,*]

Electrodes with carbon-free architecture impart a sustainable solution by eliminating side reactions. Such designs are required for anode systems especially for sodium-ion batteries where the capacity contribution from carbon is noticed additionally. Herein, carbon-free TiO_2 is prepared in the monolithic dendritic form *via* facile single-step aerosol vapour deposition technique, grown onto stainless steel current collector. The single crystalline nature of that anatase dendrites provides detailed crystallographic introspection, explicitly. Herein, we have realised an escalation of rutile phase with the existing anatase, upon cycling which is depicted as Moiré pattern while evaluating through TEM study. As the anode is carbon and binder-free, the overall material is electrochemically active, hence improves the volumetric energy-density, appreciably. Here, we perceive a long cycle life of 1000 durations from the additive-free anatase dendrite with an adequate capacity retention of 85.1%. Therefore, we believe, our single-step fabrication process to procure additive-free monolithic electrode is the forthcoming paramount technique to produce sodium-ion battery in mass.

Introduction

Devising sodium-ion battery (SIB) is one of most topical interest in current material research.[1] While sodium-ion battery produces comparatively low energy-dense systems;[2] making the electrode carbon and binder-free is noteworthy to reach the specifications of state-of-the-art lithium technology, as electrodes contain only active materials.[3] Currently, sodium electrochemistry is scavenging a durable anode while the other half, the cathode materials like $Na_3V_2(PO_4)_3$,[4] Prussian Blue[5] have been adequately ameliorated to meet the requirements of energy density as well as durability. Lithium electrochemistry has mainly commercialized four anodes: graphite,[6] $Li_4Ti_5O_{12}$,[7] Sn[8] and TiO_2[9]. However, carbonaceous anodes are still unsuccessful to deliver adequate durability over 1000 cycles at high rate, impeding rapid capacity fading.[1] Hence, TiO_2 becomes the spotlight of current research. TiO_2 is well-known as a high-rate and durable anode for lithium-ion battery, whereas ensuing similar performance with sodium systems[10-12] become a tangible challenge due to sluggish kinetics of Na-ion.[13]

Looking up recent literature, it can be realized that the TiO_2 has been studied as an anode for sodium-ion battery effectuating the concept of making binder and carbon-free electrode.[9] In relevance, we have found that carbon additive has an electrochemical property to adsorb sodium onto its surface.[10] Also, this storage property has low durability which might affect the overall battery performance. Hence, the absence of carbon also unveils the actual electrochemical outcome facilitating a high durability. Still, the rate performance of these carbon and binder-free systems need improved capacity upshot. Studies conducted from Tarascon's group[3] and from Yi Cui's group[14] showed that columnar type morphologies facilitate to avail more surface area of the active materials. Modifying such ideas, an electrode can be sculpted in a monolithic form which reduces the volume of extended current collector maintaining a well-defined particle-particle connection. In addition, ample space is required for the electrolyte to avail the active material interface for storage reactions. This can be achieved by making a nano-pillar grown perpendicular to the current collector.[15] In a nutshell, a fossilized columnar dendritic morphology[16, 17] is ideal to generate a high energy-density along with an improved rate performance.

Presently, we report monolithic dendritic TiO_2 growth material as anode for sodium-ion battery, for the first time. Using a one-step aerosol chemical vapour deposition (ACVD) process we have grown the dendritic morphology on stainless-steel current collector, used further as the electrode. Upon rate cycling followed by a prolonged run till 1000 cycles, a retention in morphology has been observed depicting a structural benefit of the procured structure. Here, a long-term cycling till 1000 cycles is reported for the first time for monolithic TiO_2, in the case of SIB. Interestingly, the one-dimensional grown anatase TiO_2 explicitly reveal a phase change to rutile upon

[a] *Aerosol and Air Quality Research Laboratory, Department of Energy, Environmental and Chemical Engineering, Washington University in St. Louis, St. Louis, MO 63130, USA.*
[b.] *Electrochemical Energy Laboratory, Department of Energy Science and Engineering, Indian Institute of Technology Bombay, Mumbai - 400076, India.*
[#]These authors contributed equally.
Electronic Supplementary Information (ESI) available: [details of any supplementary information available should be included here]. See DOI: 10.1039/x0xx00000x

cycling. In the current study, the phase change has been looked into in detail *via ex-situ* XRD, TEM, XPS and Raman studies. For the first time in case of sodium-ion anode, a rotational Moirè fringe has been observed upon sodium-ion insertion. We believe, the concept involving in the one-step electrode fabrication deploying towards a tolerable dendritic morphology will enrich the next generation research of metal-ion batteries.

Experimental Section

Synthesis of TiO_2 Electrode

TiO_2 nanostructures were synthesized using the single-step ACVD process.[17, 18] Vapors of titanium tetraisopropoxide at a concentration of 1.29×10^{-3} mol m^{-3} were introduced into the reactor where they thermally decomposed to form TiO_2 molecules which nucleated and grew to form particles. These particles were deposited onto a 1 cm diameter stainless steel substrate (25 µm thickness) maintained at 500 °C, on which the particles sintered to form 1D columnar nanostructures. The deposition was carried out for 30 min.

Materials Characterization

The morphology of the nanostructures was analyzed using field emission gun scanning electron microscopy (FEGSEM, NOVA NanoSEM 230, FEI Co.), and the crystal structure was characterized using X-ray diffraction (XRD) (Bruker D8 Advance) with CuKα radiation (wavelength = 1.5406 Å) at 35 kV and 35 mA. The scattering angle (2θ) was from 20° to 60°, with a step size of 0.02° and a dwell time of 2 sec. Rietveld refinement to obtain the lattice parameters from the XRD spectra was carried out using Topas 5 software (Bruker). Before and after cycling, detailed studies of crystal orientation, selected area electron diffraction (SAED) and morphology studies were done with high-resolution transmission electron microscopy (HR-TEM, JEOL J2100F) operated at 200 kV.

Electrochemical Cell Fabrication and Measurements

Anatase TiO_2, deposited on a stainless-steel substrate with a diameter of 1 cm, was used as a working electrode (WE) to study the electrochemical behavior of TiO_2 as an electrode for Na-ion batteries. Galvanostatic charge-discharge tests were carried out using a lab scale Swagelok type stainless steel setup, having a cell configuration of Na|electrolyte|TiO_2. All electrochemical cells were assembled in an argon-filled glovebox (Lab Star, MBraun, Germany) under controlled moisture and oxygen concentrations below 1 ppm. Na foil (Alfa Aesar, 99.8%) was used as the counter electrode as well as the reference electrode (CE/RE). Electrolyte preparation for this study was done inside the glove box. A solution (EC:PC) of ethylene carbonate (EC) (Sigma, 98%) and propylene carbonate (PC) (Sigma, 99.7% anhydrous), in a 1:1 volume ratio was prepared. $NaClO_4$ salt (Sigma, 98%), which was vacuum dried for two days and inserted into the glove box, was dissolved into the EC:PC solution to achieve a 1 M concentration. This solution was used as the electrolyte. The separator was a porous borosilicate glass microfiber filter (Whatman), soaked with a few drops of the electrolyte. Electrochemical charge-discharge experiments were performed to evaluate the durability of the prepared cells, using an Arbin battery testing instrument (BT2000, USA) at various constant current rates. Potentiostatic electrochemical impedance spectroscopy (PEIS) was carried out for the first discharge cycle using a Bio-Logic VMP-3 electrochemistry workstation. The technique was performed within a frequency range of 1 MHz to 1 Hz and with a voltage amplitude of ΔV = 10 mV. Further, the galvanostatic intermittent titration technique (GITT) was used to study the kinetics of Na-ion diffusion into the TiO_2 matrix. These electrochemical experiments were carried out at a constant current density of 50 mA g^{-1} keeping a constant temperature of 20 °C.

Ex-situ analysis

Ex-situ analysis of the cycled electrodes was carried out using XRD, Raman spectroscopy, X-Ray photoelectron spectroscopy (XPS), HR-TEM, SAED, and scanning transmission electron microscopy – energy dispersive X-ray spectroscopy (STEM-EDX) to examine the structural changes in the nanocolumns upon Na-ion insertion and de-insertion. Raman spectroscopy (using HOBIBA LabRAM HR 800 spectrometer having 532 nm solid-state laser source of 50 mW) confirmed the composition of the electrode using 100x lens with 10% edge filter. STEM-EDX analysis was carried out in the HR-TEM instrument at the operating parameters mentioned previously. Line scan EDX analysis was conducted along the length and the width of the column. XPS measurements were carried out using a PHI 5000 VersaProbe II equipped with monochromatic Al Kα (1486.6 eV) X-ray source. Fine scans were done for Na, Ti, C, and O. XPS peak analysis was done using Multipack (v9.6, ULVAC-PHI), and peaks were fitted to a Gaussian-Lorentzian mixed function via the iterated Shirley method. The peaks were calibrated using the peak for adventitious surface carbon at 284.80 eV, corresponding to C 1s photoemission. These *ex-situ* experiments were carried out by cycling the cells at 50 mA g^{-1} current rate. In addition, few more *ex-situ* characterizations were performed after 1000 cycles where the cell was at de-sodiated state.

Results and Discussion

Electrode Fabrication and Rate Cycling

Carbon and binder-free monolithic anatase TiO_2 dendrites were directly grown on the stainless steel current collector in a single-step ACVD process as shown in Figure 1a. We have previously elucidated the formation mechanism of different morphologies that can be synthesised by the ACVD process.[19, 20] The procured morphology was columnar in structure which favour adequate interfacial area for the electrolyte.[17] The fabricated electrodes were subjected to discharge-recharge at different rates for first 30 cycles (Figure 1b). The as-prepared electro-active material exhibits 357 mAh g^{-1} (2^{nd} cycle), 223 mAh g^{-1} (6^{th} cycle), 180 mAh g^{-1} (11^{th} cycle), 151 mAh g^{-1} (16^{th} cycle), 115 mAh g^{-1} (21^{st} cycle), and 89 mAh g^{-1} (26^{th} cycle) discharge capacities and 180 mAh g^{-1} (2^{nd} cycle), 177 mAh g^{-1} (6^{th} cycle), 156 mAh g^{-1} (11^{th} cycle), 136 mAh g^{-1} (16^{th} cycle),

105 mAh g^{-1} (21st cycle), and 83 mAh g^{-1} (26th cycle) charge capacities at constant current rates of 20 mA g^{-1} (0.06 C), 50 mA g^{-1}, 100 mA g^{-1} , 200 mA g^{-1}, 500 mA g^{-1}, and 1000 mA g^{-1} (3 C), respectively. After the initial rate cycling, the performance was prolonged till 1000 cycles at 100 mA g^{-1} current rate. At 1000th cycle, the TiO_2 columns exhibited a discharge capacity of 120 mAh g^{-1}, thus retaining 85.1% capacity with respect to the 31st cycle (141 mAh g^{-1}). At the end of 1000 cycles, the cell was disassembled and subjected to different physical characterizations. Here, we have compared the morphology of the TiO_2 columns after 1000 cycles with the as-prepared material. Subsequently, a retention in morphology has been explicitly depicted through SEM study (Figure 1c). In addition, TEM study also shows retention of columnar morphology (Figure 1d) after 1000 cycles when looked up for a single column. However, the single-crystalline TiO_2 become polycrystalline after cycling which has been discussed in detail in the Supplementary Information (Figure S2).

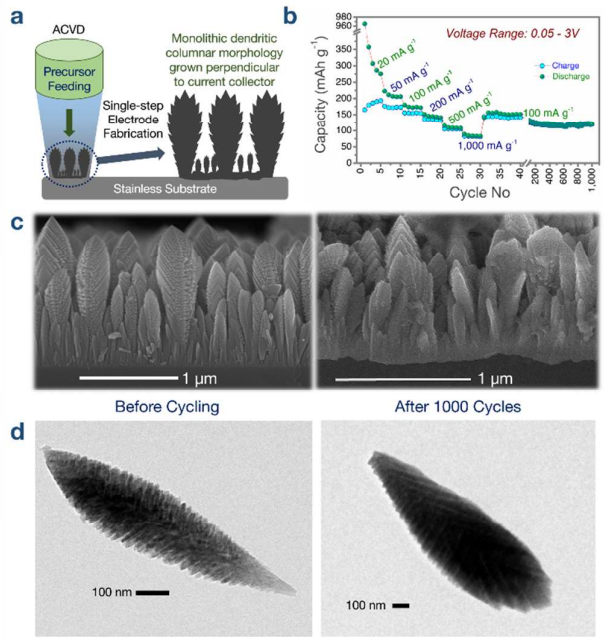

Fig. 1. (a) Synthesis pathway, (b) cycling performance and morphological comparison of TiO_2 through (c) SEM, (d) TEM for as-prepared and after 1000 cycles.

Electrochemistry

To evaluate the reactions at different voltages with respect to Na/Na^+, the dQ/dV [d(capacity)/d(voltage)] for different cycles at varying current rates was plotted (Figure 2a). Initial cycling and GITT at the 2nd cycle, have been elaborated in Supplementary Information (Figure S3). In this part, only extended cycling at 100 mA g^{-1} has been described. Two prominent reduction peaks were observed during the reduction process in all cycles. The peak near 0.74 V vs. Na/Na^+ can be attributed to Na-ion insertion into the TiO_2 host matrix. Vice versa, de-insertion of Na-ions from the TiO_2 was observed in the oxidation cycles near 0.78 V vs. Na/Na^+.[21] The as-prepared material exhibited an excellent reversibility of 99.55% at the 1000th cycle (Table T1, Supplementary Information). The potential difference obtained from the dQ/dV plot was observed to be 41 mV (at 1000th cycle) taking Na-ion insertion peak at 0.738V and a Na-ion de-insertion peak at 0.779 V. In average, the overall battery performs near 0.76 V.

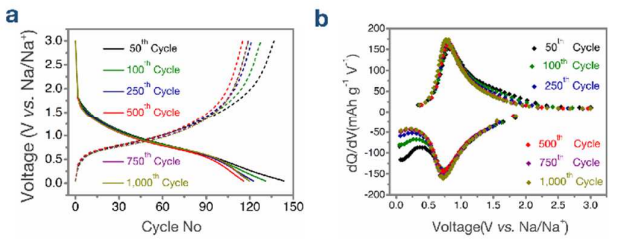

Fig. 2. (a) Charge-discharge performance and (b) dQ|dV plots at the extended cycling.

Structural and Phase Change upon Cycling

In this part, we have aimed to map the mechanism of reversible Na-ion storage into the single-crystalline anatase TiO_2. Here, *ex-situ* XRD, XPS, Raman and TEM studies were performed on the cycled electrodes. Initially, *ex-situ* was performed at discharged (0.05 V) and charged state (3 V) for the 1st and 2nd cycle. With the obtained X-ray diffraction patterns (Figure 3a) lattice parameters (a, c) were measured for the cycled electrodes and compared with the pristine TiO_2. A slight increase in lattice constants was also observed for all the cycled TiO_2 samples, as compared to the pristine TiO_2 samples (Figure 3b). Going from pristine to the first sodiation, both unit cell parameters, *a* and *c*, increase from 3.7845 Å to 3.7868 Å and from 9.4957 Å to 9.5027 Å, respectively. This expansion is consistent with previously reported detailed *in-situ* and *ex-situ* XRD analyses for Li and Na-ion intercalation into anatase TiO_2.[22, 23] After the first insertion, the lattice parameters changed in well-defined trend. After the charge, *a* increases and *c* decrease; while the opposite phenomenon happened after discharge. Here, lattice constants of the tetragonal crystal structure (I41/amd) obtained via Rietveld refinement of the XRD spectra of pristine TiO_2 and cycled TiO_2 samples. For this typical calculation, anatase standard diffraction pattern was taken from ICSD PDF No. 01-071-1166 and the rutile standard diffraction pattern was taken from ICSD PDF No. 04-001-7096. *Ex-situ* XPS study on cycled electrodes (Figure 3c) shows the presence of Ti^{3+} after discharge which was disappeared after charge. The peak at 457.64 eV corresponds to the Ti^{3+} binding energy, while the 458.53 eV corresponds to the Ti^{4+} binding energy.[24] This reflects the Na-ion insertion into the lattice which is quite similar to Li electrochemistry.[25] Interestingly, Raman study after 1000 cycles (Figure 3d) shows an additional phase of rutile subsumed with anatase. The *ex-situ* Raman study has been discussed in the Supporting Information (Figure S5). The

presence of rutile was also depicted through X-ray diffraction pattern (Figure 3d inset), in which (1 1 0) plane of rutile phase was explicitly observed. It was assessed that the change in lattice parameters upon cycling and the occurrence of rutile phase can culminate a mechanistic pathway of Na-ion insertion and de-insertion into the TiO_2 matrix.

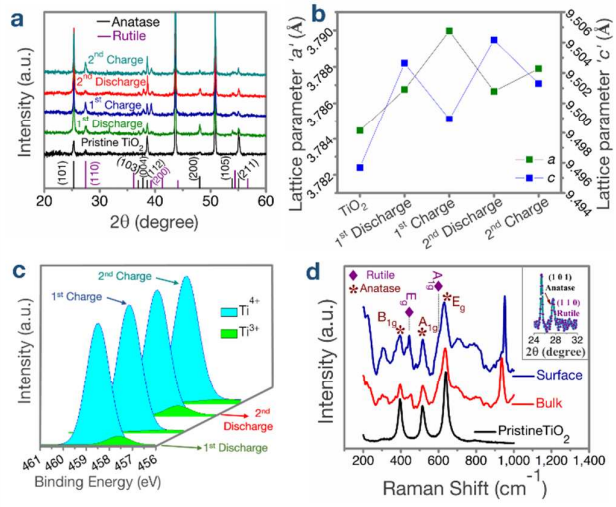

Fig. 3. *Ex-situ* (a) XRD and corresponding (b) lattice parameters analyses and (c) XPS of the nanostructured TiO_2 anode during the first two charge and discharge cycles., (d) *Ex-situ* Raman after 1000 cycles; inset: XRD after 1000 cycles.

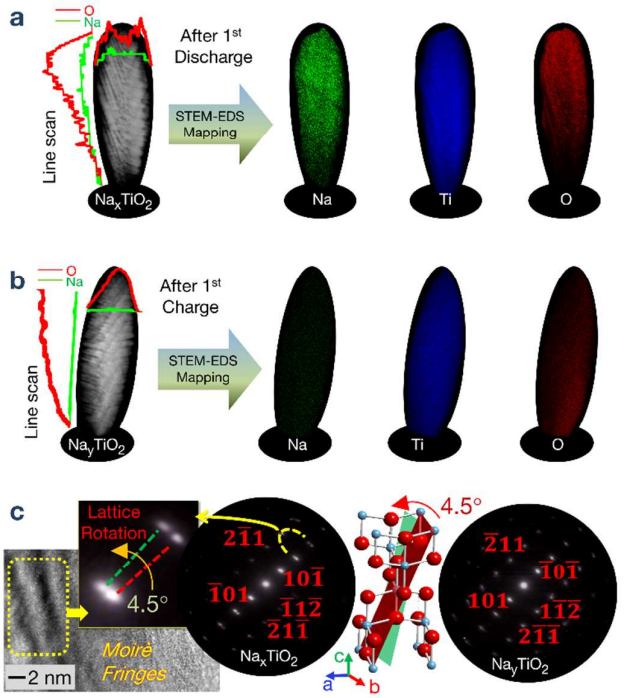

Fig. 4. STEM-EDX mapping of TiO_2 columns after (a) 1st discharge, (b) 1st charge along with line scan data for the same columns with the (c) SAED pattern and HR-TEM image to evaluate the Na-ion storage.

To scrutinize in detail, the first sodiated and de-sodiated electrodes were subjected to TEM analysis. Initially, a mapping study was performed onto these two electrodes. For this typical study, the surface adsorbed sodium compounds were removed with water which has been detailed in the Supporting Information (Figure S6). An SETM-EDS map of Na, Ti and O were carried out. This show that Na was well distributed throughout the column while discharging and purged out in a uniform manner after charging. To support more, line scans were performed with the same single columns across the width and length of the column. This also depicts the similar distribution. In the next step, SEAD pattern of these electrodes was compared fixing the zone axis to (*h* 0 *l*) direction. A fascinating outcome was noticed explicitly through this study. For the first time, a rotational Moirè fringe patterns observed on the column surface for the sodiated samples (Figure 4c) suggest the presence of two overlaying lattices. The observed rotation for this typical case was 4.5°. This phenomenon occurred after Na-ion insertion into the TiO_2 matrix and disappeared after charging. This part has been further described in Supplementary Information (Figure S7).

Brief Discussion

Initially, this study focuses on the morphological benefit of the monolithic dendrites while used as carbon and binder-free electrode for Na-ion battery. We have recently reported that a significant capacity is contributed by conductive carbon in the potential range of 0.01-1 V. Therefore, in current study, we have used a carbon-binder free to judge the actual capacity contribution from the electrode. The advantage of this morphology is the well-defined connection between grown columns and the current collector and the separation between columns helps electrolyte to access the electrolyte-electrode interface. Hence, a homogeneous surface reaction occurs (observed through STEM-EDS mapping, Figure 4 a, b). However, these additive-free electrodes need an initial activation (reaction) to rearrange the crystallinity facilitating towards easy Na-ion insertion and de-insertion. This assessment is reflected in an improvement in capacity while cycling was initially performed at a very slow rate (20 mA g^{-1}) in comparison with a higher rate (discussed in Supplementary Information, Figure S1). At the time of slow rate cycling, for first two cycles, the obtained capacity output was higher than the theoretical capacity (335 mAh g^{-1})[11] which is most likely due to the surface adsorption of Na-compounds onto the surface. This appraisal has been reflected at the time of STEM-EDS mapping, XPS and in PEIS study (discussed in Supplementary Information, Figure S4). In addition, a stable electrolytic resistance (~13.35 Ω) were obtained from PEIS

study (discussed extensively in Supplementary Information, Figure S4). After the first discharge, the *ex-situ* SEM does not show any additional morphology as observed from Passerini's group.[25] This observation reflects that additional morphology was coming from reaction with conductive carbon which is in computability with our previous study on conductive carbon.[26] Hence, this carbon-free system does offer an easy-fuelling of Na-ion at the interface which resulted in a long-term cycling till 1000 cycles. Interestingly, GITT study shows that the diffusion co-efficient ($8.54x10^{-18}$ cm^2 s^{-1}) is ~20 times than the previously reported additive-free TiO_2 (discussed extensively in Supplementary Information, Figure S3 d).[15] Although, the overall electrochemical outcome is similar to lithium, but differs significantly from the operational voltage. Generally, TiO_2 performs near 1.5-1.6 V *vs.,* Li/Li_+;[17] while the same material performs at much lower potential (~ 0.76 V). It is well known that a low-voltage anode results in enhanced energy-density and power-density.[2] Therefore, the removal of unnecessary components from electrode volume and the lower potential operation significantly improves the volumetric energy-density, which is the rudimentary requisite to ameliorate sodium electrochemistry. In comparison with similar reports on TiO_2, our anatase dendrites performs quite better in terms of capacity. Nearly, 30% improvement in specific capacity has been observed which has been detailed in Figure S8 (Supporting information).

As the material is 1D-grown anatase TiO_2, hence the structural and phase changes were noticed explicitly through *ex-situ* studies. The insertion of Na-ion into TiO_2 matrix affects the (*h* 0 *l*) direction and produces a distorted lattice which reflects as a lattice rotation (depicted as Moiré fridge in SAED, Figure 4c). Probably, an amount of stain gets induced into the TiO_2 lattice. While oxidation (de-insertion of Na-ion), the material seeks to retain its original structure to anatase. Interestingly, the crystalline structure does not back to the exact pristine TiO_2. This phenomenon has been observed as the initial increment in lattice parameters (*a* and *c*) which does not decrease to its original value even after de-sodiated state. Initially, the material induces strain due to sodiation which reflected as Moiré pattern. After de-sodiation, the strain releases and the material incorporates rutile phase along with anatase. Upon cycling, the single-crystalline TiO_2 become polycrystalline (discussed extensively in Supplementary Information, Figure S2) and keeps the additional rutile phase retaining the initial morphology. As a result, after de-sodiations (after 1^{st}, 2^{nd}, 1000^{th} etc.) the X-ray diffraction patterns and Raman spectra show the presence of rutile phase along with the anatase phase.

Conclusion

In summary, for the first time, a monolithic anatase TiO_2 electrode has been proposed as a binder and conductive carbon-free anode for sodium-ion battery. Here, TiO_2 exhibits a long cycle life of 1000 including initial rate cycling, without changing its preparatory morphology. The retention in capacity is 81.5% with a high Coulombic efficiency of 99.55% (at 1000^{th} cycle). Na-ion insertion and de-insertion happen near 0.76 V, which is a significant advantage as Na-ion battery anode over currently used lithium system. *Ex-situ* SEM, TEM, XRD and XPS confirms about the additional phase incorporation of rutile after cycling. From SAED, a rotational Moiré pattern has been described, for the first time to describe Na-ion insertion into an anode system. Our collaborative study on single-step monolithic additive-free electrode fabrication at both Washington University in St. Louis and the Indian Institute of Technology Bombay, addressing a long-term durability is on its way to monetize in attenuated devices like a pacemaker, smart watches etc. Currently, we are working on further improving the specific capacity by introducing significant dopant in a cost-effective way and developing scaleup roll to roll ACVD process for large scale manufacturing and maintaining an environmental benignity.

Conflicts of interest

There are no conflicts of interest to declare.

Author Contributions

[#]These authors contributed equally. TSC, PKD, SM and PB designed the study. TSC and PKD carried out the synthesis of the nanostructured anode and the electrochemical characterization. RR aided with the XPS and TEM measurements. TSC and PKD wrote the manuscript, SM and PB revised it and all authors approved the final version before submission. SM and PB provided the overall supervision on this project.

Acknowledgements

This paper is based upon work supported by the Solar Energy Research Institute for India and the U.S. (SERIIUS) funded jointly by the U.S. Department of Energy subcontract DE AC36-08G028308 (Office of Science, Office of Basic Energy Sciences, and Energy Efficiency and Renewable Energy, Solar Energy Technology Program, with support from the Office of International Affairs) and the Government of India subcontract IUSSTF/JCERDC-SERIIUS/2012 dated 22nd Nov. 2012. The authors acknowledge Dr. Huafang Li at the Institute of Material Science and Engineering (IMSE), Washington University in St. Louis for help with STEM measurements and Professor James C. Ballard for reviewing the manuscript.

Notes and references

1 M. D. Slater, D. Kim, E. Lee and C. S. Johnson, *Adv. Funct. Mater.*, 2013, **23**, 947-958.

2 V. Palomares, P. Serras, I. Villaluenga, K. B. Hueso, J. Carretero-Gonzalez and T. Rojo, *Energy Environ. Sci.*, 2012, **5**, 5884-5901.
3 P. L. Taberna, S. Mitra, P. Poizot, P. Simon and J. M. Tarascon, *Nat. Mater.*, 2006, **5**, 567-573.
4 Y. Xu, Q. Wei, C. Xu, Q. Li, Q. An, P. Zhang, J. Sheng, L. Zhou and L. Mai, *Adv. Energy Mater.*, 2016, **6**, 1600389-n/a.
5 Y. Jiang, S. Yu, B. Wang, Y. Li, W. Sun, Y. Lu, M. Yan, B. Song and S. Dou, *Adv. Funct. Mater.*, 2016, **26**, 5315-5321.
6 J. O. Besenhard and G. Eichinger, *J. Electroanal. Chem. Interfacial Electrochem.*, 1976, **68**, 1-18.
7 X. Han, M. Ouyang, L. Lu and J. Li, *Energies*, 2014, **7**, 4895-4909.
8 W. M. Zhang, J. S. Hu, Y. G. Guo, S. F. Zheng, L. S. Zhong, W. G. Song and L. J. Wan, *Adv. Mater.*, 2008, **20**, 1160-1165.
9 D. Wang, D. Choi, J. Li, Z. Yang, Z. Nie, R. Kou, D. Hu, C. Wang, L. V. Saraf and J. Zhang, *ACS Nano*, 2009, **3**, 907-914.
10 J.-Y. Hwang, S.-T. Myung and Y.-K. Sun, *Chem. Soc. Rev.*, 2017, **46**, 3529-3614.
11 Y. Zhang, C. W. Foster, C. E. Banks, L. Shao, H. Hou, G. Zou, J. Chen, Z. Huang and X. Ji, *Adv. Mater.*, 2016, **28**, 9391-9399.
12 G. Zou, H. Hou, P. Ge, Z. Huang, G. Zhao, D. Yin and X. Ji, *Small*, 2018, **14**, 1702648.
13 D. Prutsch, M. Wilkening and I. Hanzu, *ACS Appl. Mater. Interfaces*, 2015, **7**, 25757-25769.
14 C. K. Chan, H. Peng, G. Liu, K. McIlwrath, X. F. Zhang, R. A. Huggins and Y. Cui, *Nat. Nanotech.*, 2008, **3**, 31.
15 H. Xiong, M. D. Slater, M. Balasubramanian, C. S. Johnson and T. Rajh, *J. Phys. Chem. Lett.* , 2011, **2**, 2560-2565.
16 S. Wenzel, T. Hara, J. Janek and P. Adelhelm, *Energy Environ. Sci.*, 2011, **4**, 3342-3345.
17 T. S. Chadha, A. M. Tripathi, S. Mitra and P. Biswas, *Energy Technol.*, 2014, **2**, 906-911.
18 T. S. Chadha, P. Biswas and W.-J. An, U.S. Patent Application No. 14/830,361, 2016.
19 T. S. Chadha, M. Yang, K. Haddad, V. B. Shah, S. Li and P. Biswas, *Chem. Eng. J.*, 2017, **310**, 102-113.
20 K. Haddad, A. Abokifa, S. Kavadiya, T. Chadha, P. Shetty, Y. Wang, J. Fortner and P. Biswas, *CrystEngComm*, 2016, **18**, 7544-7553.
21 Z. Le, F. Liu, P. Nie, X. Li, X. Liu, Z. Bian, G. Chen, H. B. Wu and Y. Lu, *ACS Nano*, 2017, **11**, 2952-2960.
22 K.-T. Kim, G. Ali, K. Y. Chung, C. S. Yoon, H. Yashiro, Y.-K. Sun, J. Lu, K. Amine and S.-T. Myung, *Nano Lett.*, 2014, **14**, 416-422.
23 R. van de Krol, A. Goossens and E. A. Meulenkamp, *J. Electrochem. Soc.*, 1999, **146**, 3150-3154.
24 J. Huang, D. Yuan, H. Zhang, Y. Cao, G. Li, H. Yang and X. Gao, *RSC Adv.*, 2013, **3**, 12593-12597.
25 L. Wu, D. Bresser, D. Buchholz, G. A. Giffin, C. R. Castro, A. Ochel and S. Passerini, *Adv. Energy Mater.*, 2015, **5**, 1401142-n/a.
26 P. K. Dutta and S. Mitra, *J. Power Soc.*, 2017, **349**, 152-162.

KEYWORDS. Aerosol chemical vapor deposition, binder-free anode, carbon-free electrode, electrochemistry, sodium-ion battery.

TOC

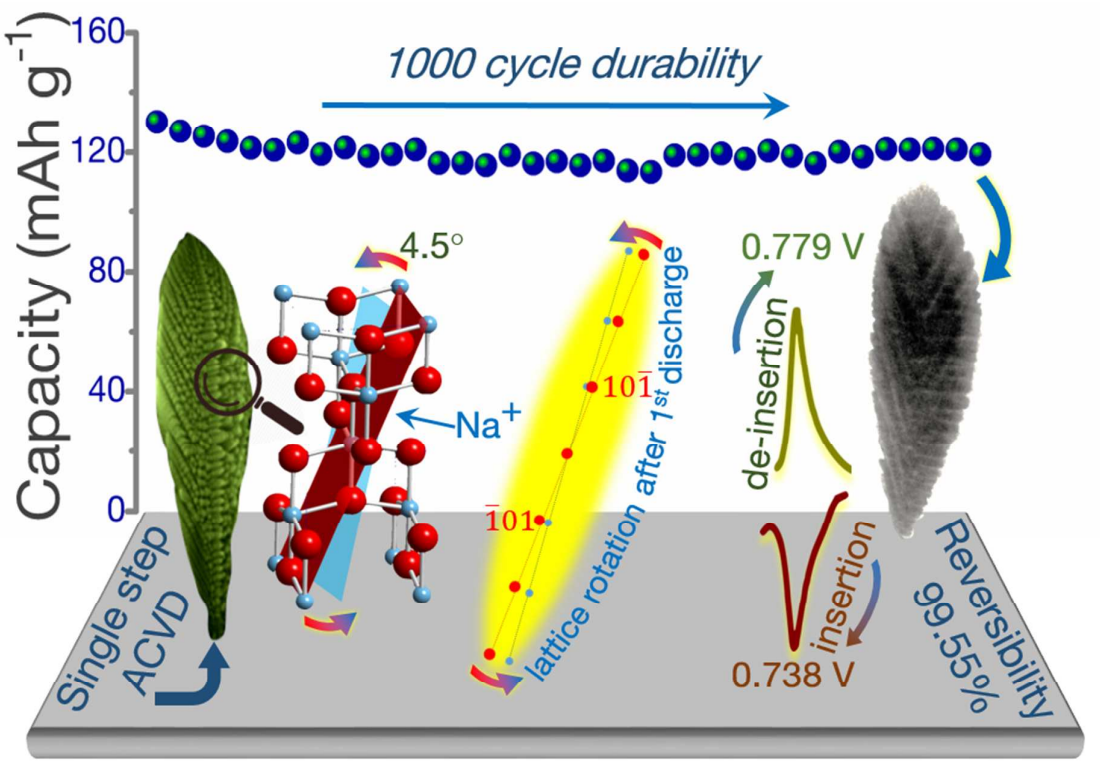

Caption:

A long-term durability of monolithic dendritic anatase TiO_2 sculptured *via* single-step ACVD technique provides a mechanistic inner-view *via* rotational Moirè pattern pursuing a 99.55% Coulombic efficiency, 41 mV polarization loss at the 1000th cycle, retaining the columnar morphology.